ISBN 82-553-0621-8 No 4
Applied Mathematics 17. Nov. 1986

BLOOD FLOW SIMULATIONS IN A CAST OF THE AORTHIC BIFURCATION

by

Arnold F. Bertelsen, Lars Wallöe
and Arve Kvalheim

PREPRINT SERIES - Matematisk institutt, Universitetet i Oslo

disk D/B

BLOOD FLOW SIMULATIONS IN A CAST OF THE AORTHIC BIFURCATION

by

Arnold F. Bertelsen*, Lars Wallöe** and Arve Kvalheim*

Abstract

The flow induced in a true conformal cast of the aorthic bifurcation, by forced steady and pulsatile inlet flows, has been investigated experimentally. It was found that the time dependent part of the inlet flow have pronounced influence on the time averaged flow down stream of the inlet. Special features of the flow field are discussed relative to localization of early atherosclerotic disease which seem to coincide with regions of low time averaged velocities close to the wall and low wall shear stress.

* - Department of Mechanics, Inst. of Math., Univ. of Oslo

** - Inst. of Informatics, Univ. of Oslo, Norway

INTRODUCTION

Atherosclerosis is a common disease in most industrialized countries. The patogenetic mechanisms of the disease is still disputed. Already in 1867 Rindfleisch launched a haemodynamic related hypothesis for the early development of atherosclerosis. He believed that particular parts of the arterial tree, such as bends and branching sites, were exposed to severe mechanical loads from the blood flow. In the last decades the mapping of arterial lesions have become more prcise and detailed which, together with advances in lipid biochemistry and fluid mechanics, have led to refined pathogenetic hypotheses of atherosclerosis. We refer to Kjærnes et al. (1981) for a more complete discussion of these hypotheses.

Haemodynamic factors are still supposed to play an important part, at least as far as the localization of the early lesions is concerned. For example, Fry (1968, 1969, 1972) postulated and verified experimentally in dog and swine that increased wall shear stress could contribute to the development of atheroma by causing an initial endothelial damage. Similar results were obtained by Roach (1983).

On the other hand, Caro (1969, 1971) suggested on the basis of some observations on human arteries, that atherosclerosis would develop in reginos with low wall shear stress. He explained this by supposing a shear dependent mass transfer rate from the wall to bulk blood flow. Fox and Hugh (1966) proposed that atherosclerotic lesions resulted from deposition of plasma constituents in the vessel wall in regions of stagnant flow.

flat cast of the bifurcation was obtained. Several intermediate casts were necessary before the final methylmetarylate model was polymerized and polished. The final model is enlarged approximately by a factor of two compared to its natural size. A sketch of the model is shown in Fig. 1 together with the coordinate systems to which the measurements are referred. The model has both the (x,y)-plane and the (y,z)-plane as symmetry planes.

2.2. The pipe flow loop

The experiments described in this paper were performed by putting the model into a recirculating pipe flow loop to obtain the requested inlet flow conditions. The flow loop is sketched in figure 2 and its main components are mentioned in the figure legend. The overhead tank gives the necessary excess mean pressure while the pump introduces the oscillatory components of the flow field. Several valves were installed to adjust the steady and oscillatory components separately in each branch. The pump forced the fluid to oscillate with a frequency stability better than 1%. The amplitude of the overharmonics as less than 3% at the inlet of the model.

2.3. Method of observation and data acquisition

The velocity field induced in the model by the overhead pressure and the oscillating piston were to some extent observed from photographic recordings, but mainly by a commercially available two component (two colour) laser Doppler anemometer (LDA) manufac-

The velocity readings were analysed using a fast Fourier transform routine (FFT) supplied by Hewlett-Packard. The Fourier coefficients together with the position readings were stored on magnetic tapes.

2.4. Data analysis and validation tests

The data (velocity readings) analysis proceeded as follows. Each sequence, say j, consisting typically of 25 samples taken in one period of the basic oscillatory motion of the fluid, was analysed by the FFT routine, giving the Fourier coefficients

$$A_{0,j}, A_{1,j}, \text{---} \quad \text{(cosine terms)}$$

and

$$B_{1,j}, B_{2,j}, \text{---} \quad \text{(sine terms)}$$

A sufficient number of sequences N were used to get standard deviations

$$\Delta A_i = \left[\frac{1}{N-1} \sum_{j=1}^{N} (A_{i,j} - A_i)^2\right]^{\frac{1}{2}}$$

$$\Delta B_i = \left[\frac{1}{N-1} \sum_{j=1}^{N} (B_{i,j} - B_i)^2\right]^{\frac{1}{2}}$$

of the mean values

$$A_i = \frac{1}{N} \sum_{j=1}^{N} A_{i,j}$$

and

$$B_i = \frac{1}{N} \sum_{j=1}^{N} B_{i,j}$$

below some chosen limits, usually a few percents. The data acquisition system and the method of analysis have been used before by Bertelsen & Thorsen (1982) and are known to work satisfactorily.

TABLE 1.

Series	Inlet flow time dependence	Mean flow Reynolds number	Mean vel.	Osc. velocity ampl.
I	Pulsatile	416	26 cm/s	36 cm/s
II	Steady	416	26 "	0
III	Pulsatile	1280	80 "	75 "
IV	Steady	1280	80 "	0

Series I and II are the most extensive, while in III and IV only a few profiles have been measured to investigate the gross effects of increasing the mean flow Reynolds number and the amplitude of the oscillations.

The measurements are presented in the following way:

1. The total velocity profiles from series I are shown in figures 4,5,6,7,8 and 9.
2. Comparison of time averaged profiles from series I with the steady profiles from series II are shown in figures 10,11,12,13,14,15,16 and 17.
3. Comparison of time averaged prifiles from series III with the steady profiles from series IV are shown in figure 18. All measurements are referred to the coordinate systems sketched in figure 1.
4. Total wall shear stress is presented in fugures 19 and 20.
5. Mean wall shear is given in Table II.

3.2. Steady and time averaged velocity profiles

To evaluate the long term effect of the unsteadiness in the problem we are modeling, time averaged profiles from series I are compared to corresponding steady profiles from series II in figures 10, 11,12,13,14,15,16 and 17. It is evident from these comparisons that the oscillatory part of the inlet flow has a pronounced influence, by non-linear interactions, on the time averaged field. For example, this can be the only explanation of the reversed time averaged axial flow at the walls of the bifurcation in series I (see figures 11 and 12). Similar effects reverse the time averaged transverse components in series I compared to the series II (see figures 15 and 16).

The same non-linear effects are observable by comparing measurements in series III and IV. This is demonstrated in figure 18 where reversed time averaged axial flow appears at the walls in the time averaged profiles when the fluid is forced to oscillate. There were no essential changes in gross features of the flow patterns by the increase in Reynolds numbers from series I & II to series III & IV, though minor differences can be observed by comparing figures 12 and 18.

We believe that the non-linear Reynolds stresses are the most important mechanism causing the alteration of the velocity profiles generated by steady inlet conditions to the corresponging time averaged profiles generated by pulsatile inlet conditions (same mean flow Reynolds number). The importance of such effects in geometries of some relevance are investigated, for example, by Lyne (1971) and Bertelsen (1982).

The velocity profiles obtained subject to steady inlet conditions compare well with those predicted by Wille (1984) using

The time averaged shear stress is given in Table 2. In this table we notice the change of direction of the mean wall shear. A region of low shear appears just above the apex, and coincides, more or less, with the location of early atherosclerotic lesions.

Table II. Mean wall shear

	x (mm)	y (mm)	z (mm)	τ (N/m^2)
Mother pipe	0	10.0	-50	0.32
	0	11.0	-20	-0.055
	0	13.2	- 5	-0.31
	x'	y'	z'	τ
Branch pipe	0	7.7	-51.5	2.79
	0	-7.7	-51.5	-0.15
	0	7.4	-38.7	0.71
	0	-7.6	-38.7	0.55

4. CONCLUSIONS

Comparing the main features of the time averaged velocities measured in this investigation to the mapping of early atherosclerotic lesions presented in figure 3 in Kjærnes, Svindland, Wallöe and Wille (1981), we can easily observe that the pattern of the lesions seems to coincide with regions of low wall shear stress and low velocities. The regions of high wall shear stress, both instantaneous peak values and time averaged values, such as the apex area, seem to be prevented from lesions. Which interaction mechanisms cause this relations cannot be discussed on the basis of these experimental results. In that context more refined models are necessary, including at least a physico-chemical model of the blood flow and the wall processes.

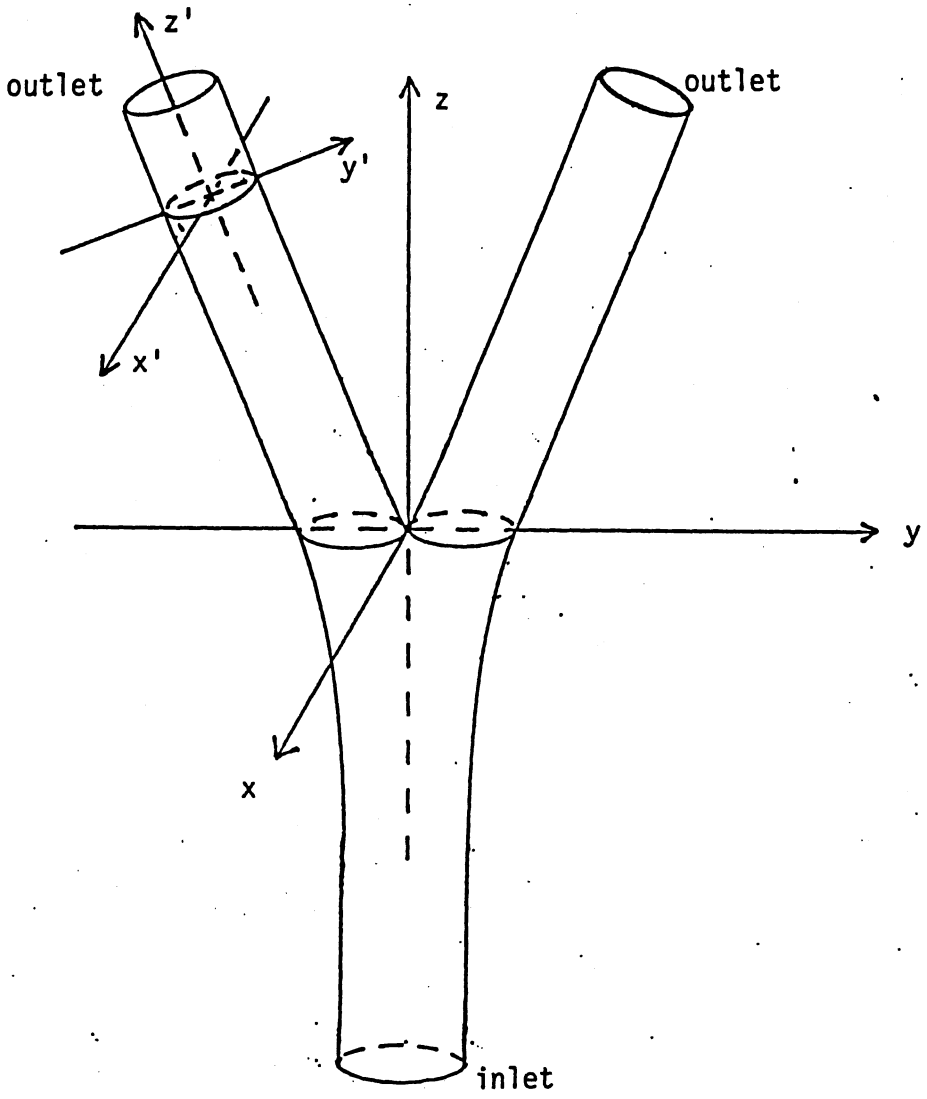

Figure 1. Sketch of the model of the aortha bifurcation and the co-ordinate systems to which the measurements are referred. $z' = -56.8$ mm at the apex point $x = y = z = 0$. Inlet diametr~20 mm, outlet diameter ~ 14.8 mm. Branching angle $\sim$ 42 deg.

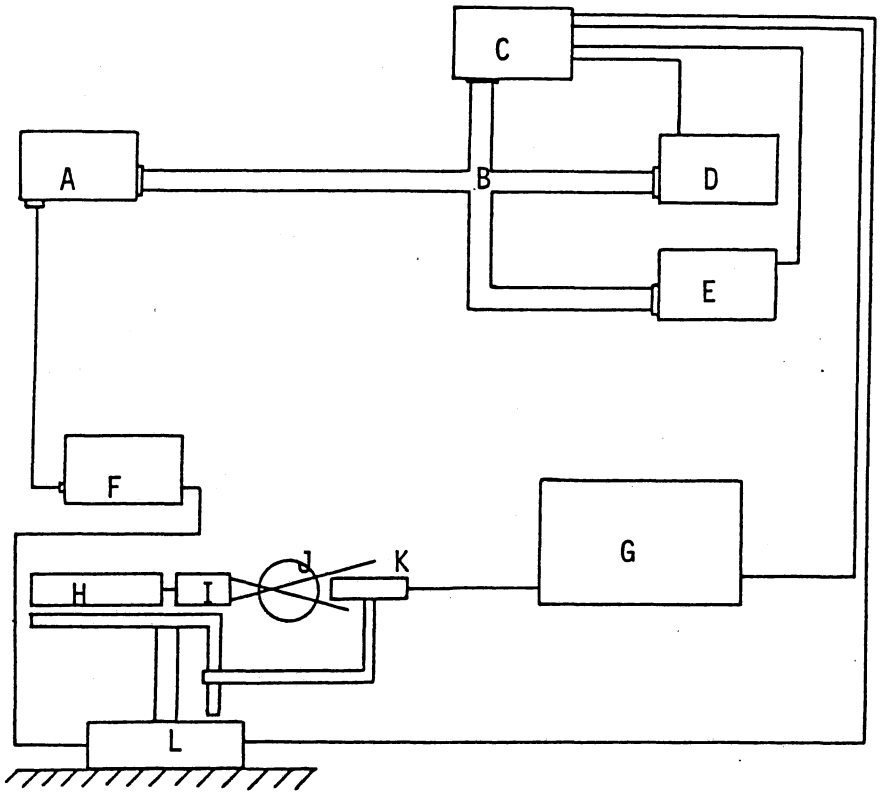

Figure 3. The main components of the laser-Doppler anemometer and the data-acquisition system: A - controller HP9825T, B - the interface bus, C - the scanner HP3495A, D - the multimeter HP3455A, E - the system voltmeter HP3437A, F - the BCD interface HP98032A, G - the Doppler signal processing equipm equipment, H - the laser, I - transmitting optics with optical modulator, J - the model, K - the photomultipliers, L - the step motors and position indicators.

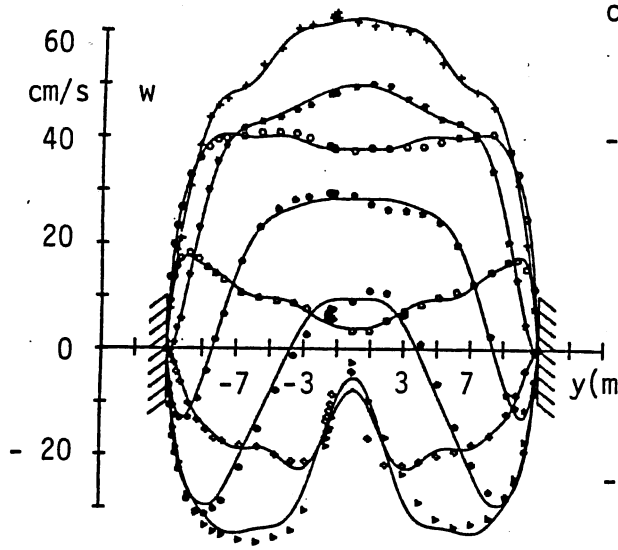

Figure 5A

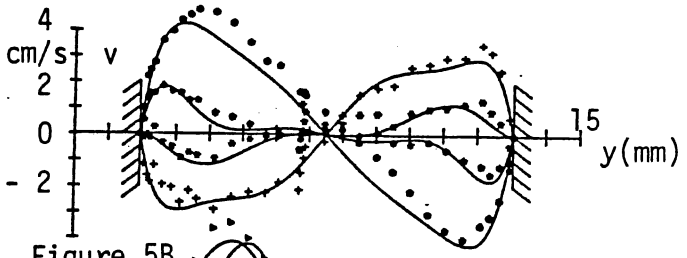

Figure 5B

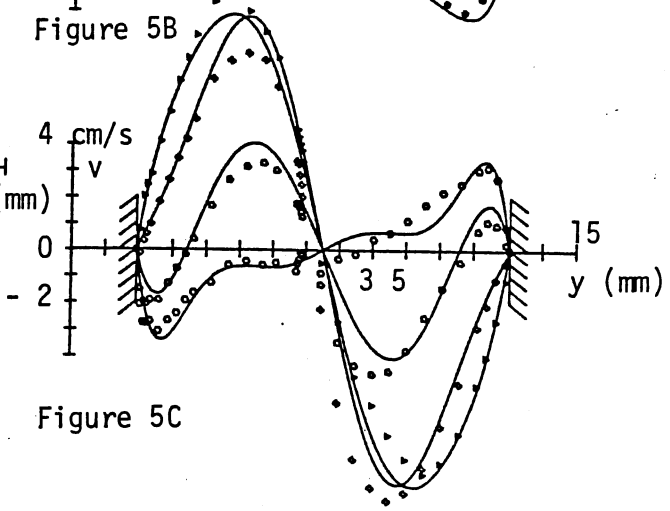

Figure 5C

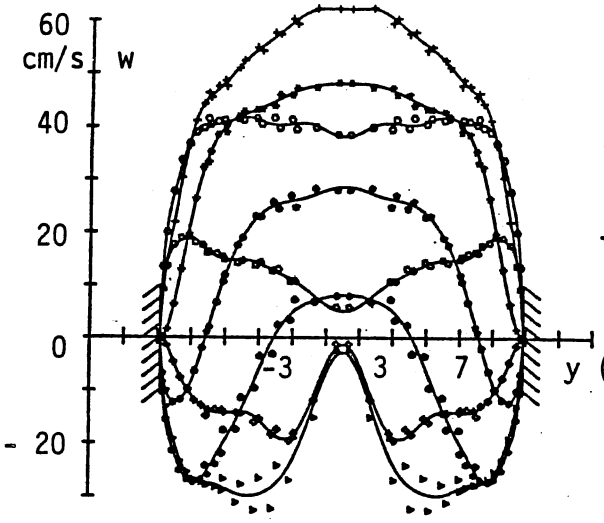

Figure 5D

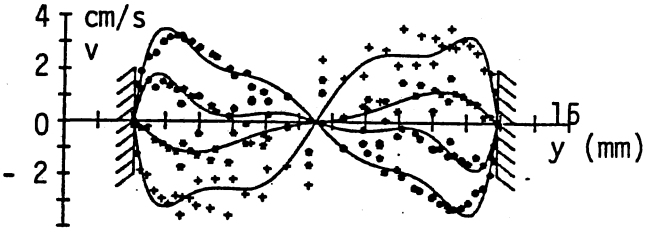

Figure 5E

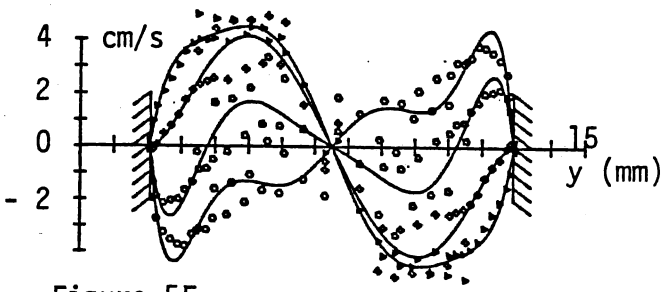

Figure 5F

Figure 5. Figure 5A show axial velocity profiles along the diameter x = 0, z = - 20mm , while 5B and C show transverse velocities (v in + y direction) along the same diameter. Figure 5D, E and F show corresponding profiles along the diameter x = 2mm, z = - 20mm.

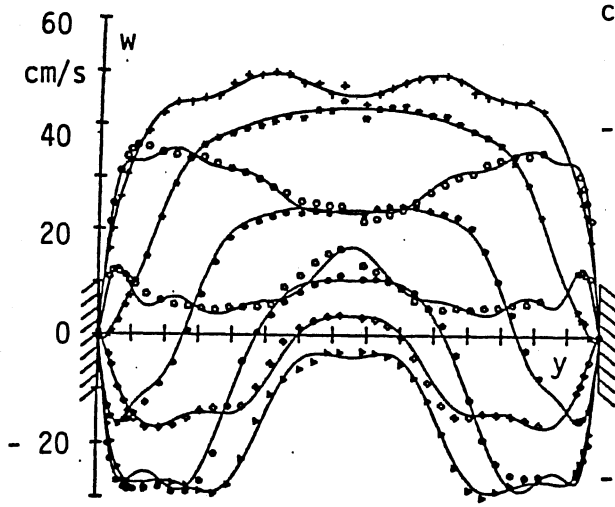

Figure 7A

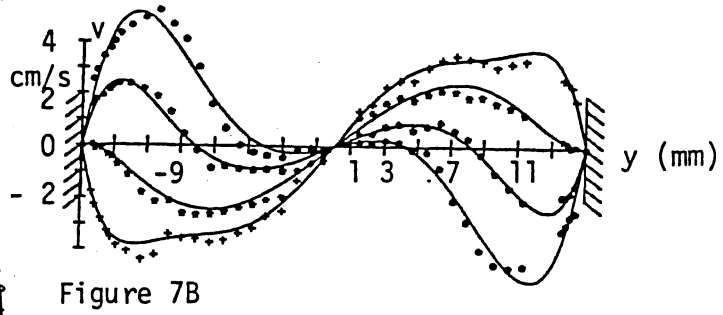

Figure 7B

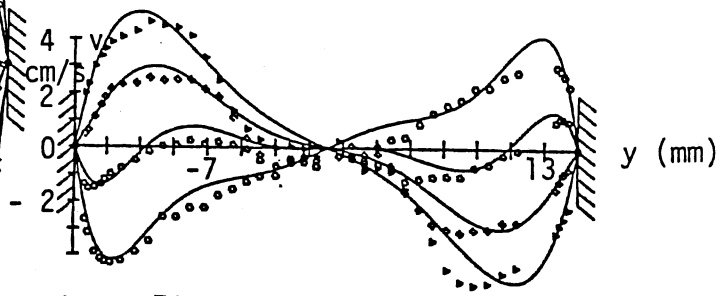

Figure 7C

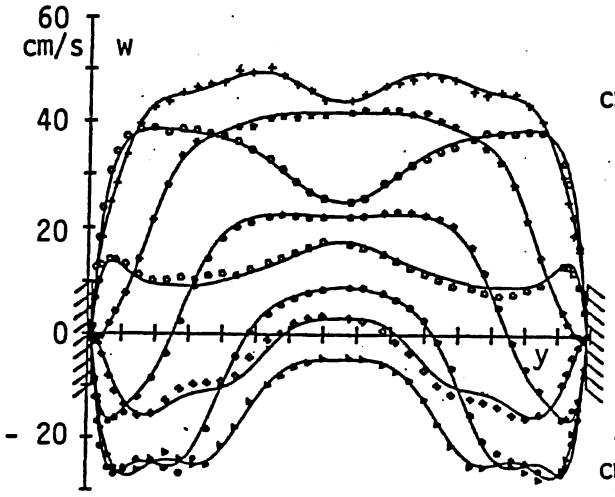

Figure 7D

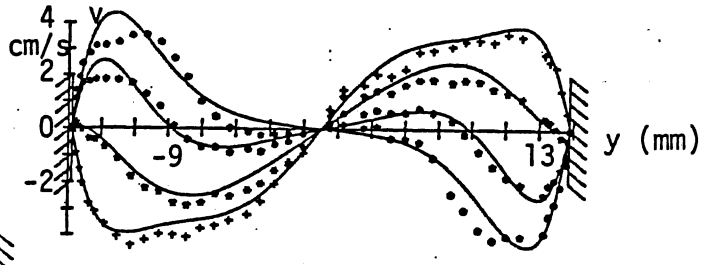

Figure 7E

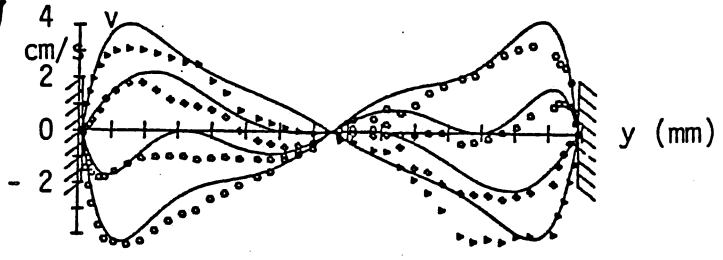

Figure 7F

Figure 7. Figure 7A show axial velocity profiles (w) at z = - 5 mm along a diameter in the yz - plane (x = 0), while 7B and C show the transverse velocity component v along the same diameter. Figure 7D, E and F show corresponding profiles at the same z-coordinate, but x = 2 mm. Symbols as in figure 4.

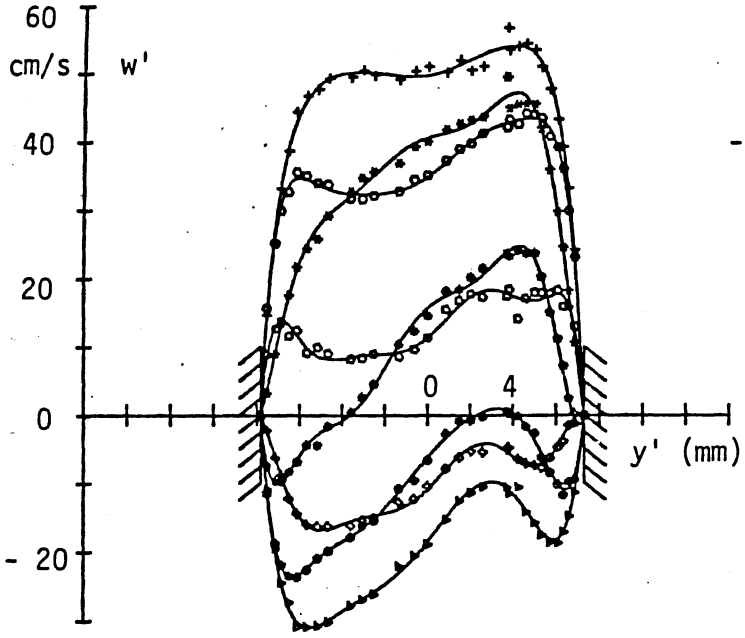

Figure 9A

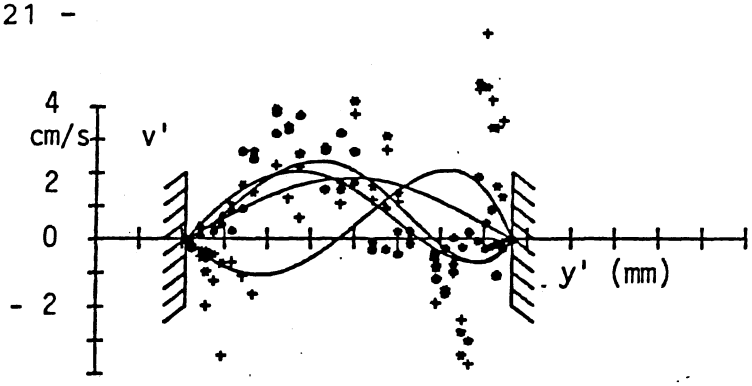

Figure 9B

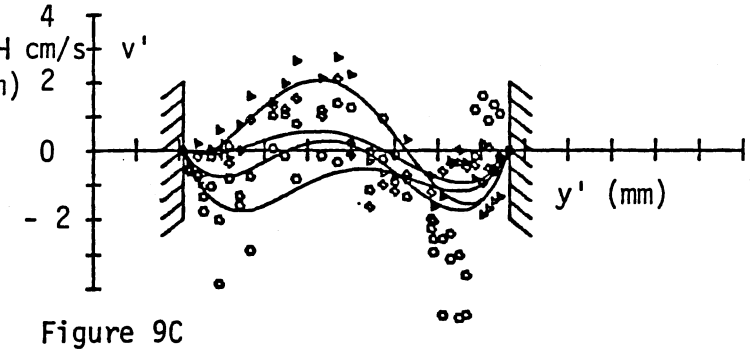

Figure 9C

Figure 9. Figure 9A show the axial velocity component w' at z' = -38.7mm along a diameter in the y'z'-plane (x' = 0), while 9B and C show the transverse velocity components v' along the same diameter.

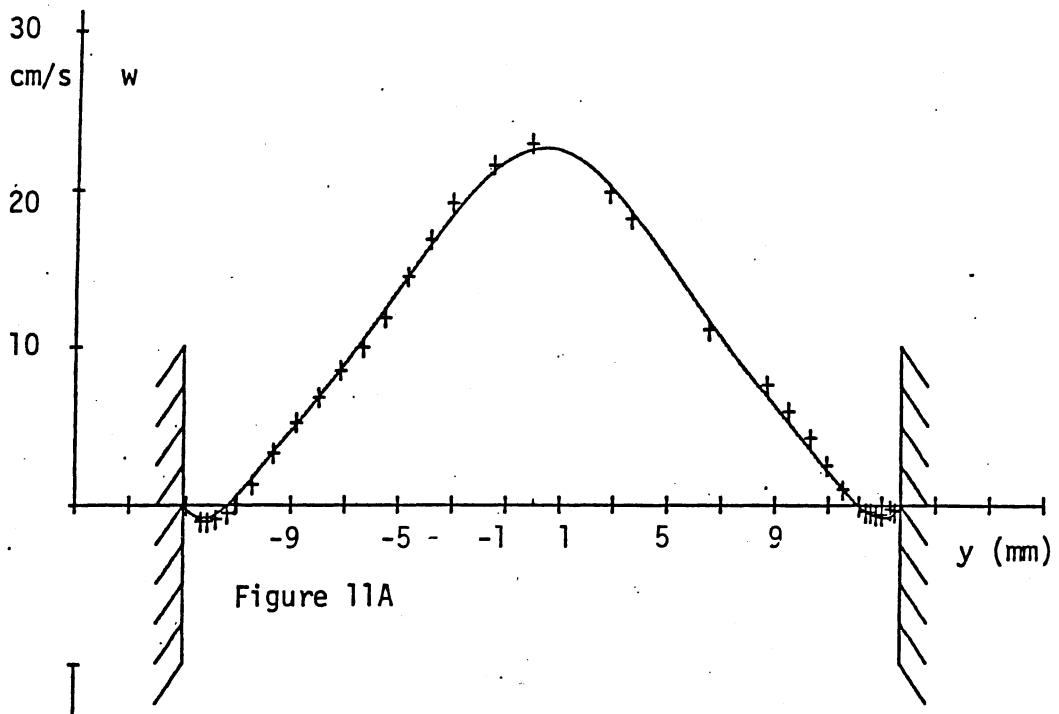

Figure 11A

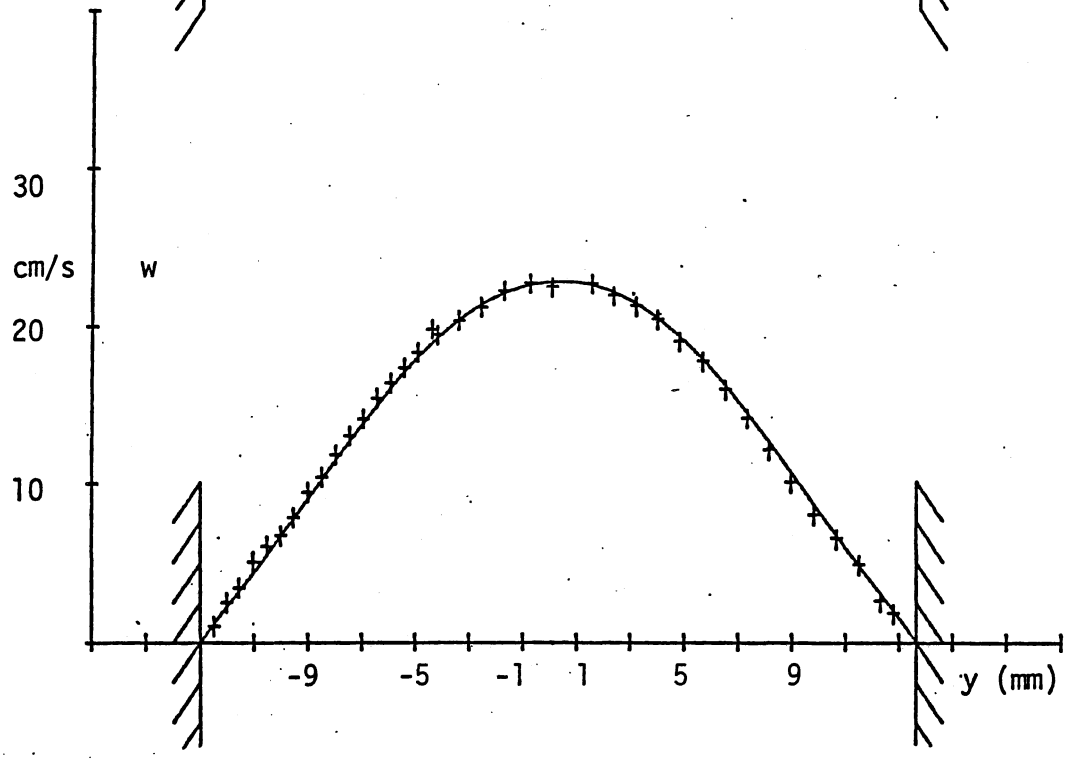

Figure 11B

Figure 11. Figure 11A show the time averaged axial velocity w in series I along a diameter in yz-plane (x = 0) at z = - 10 mm, while figure 11B is the corresponding profile from series II.

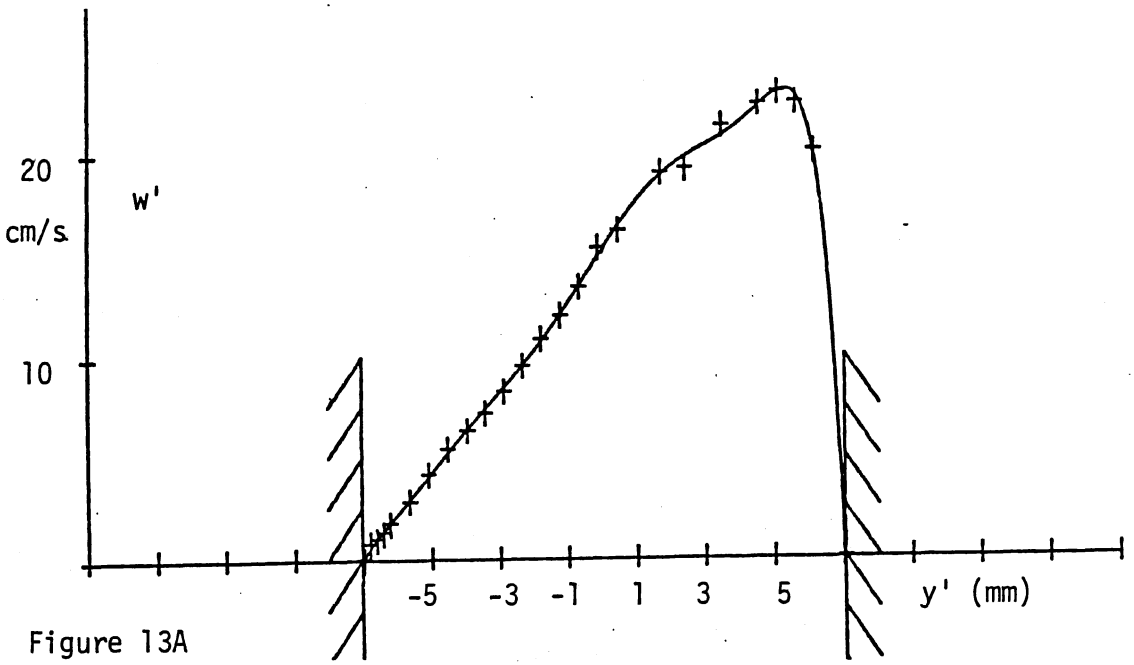

Figure 13A

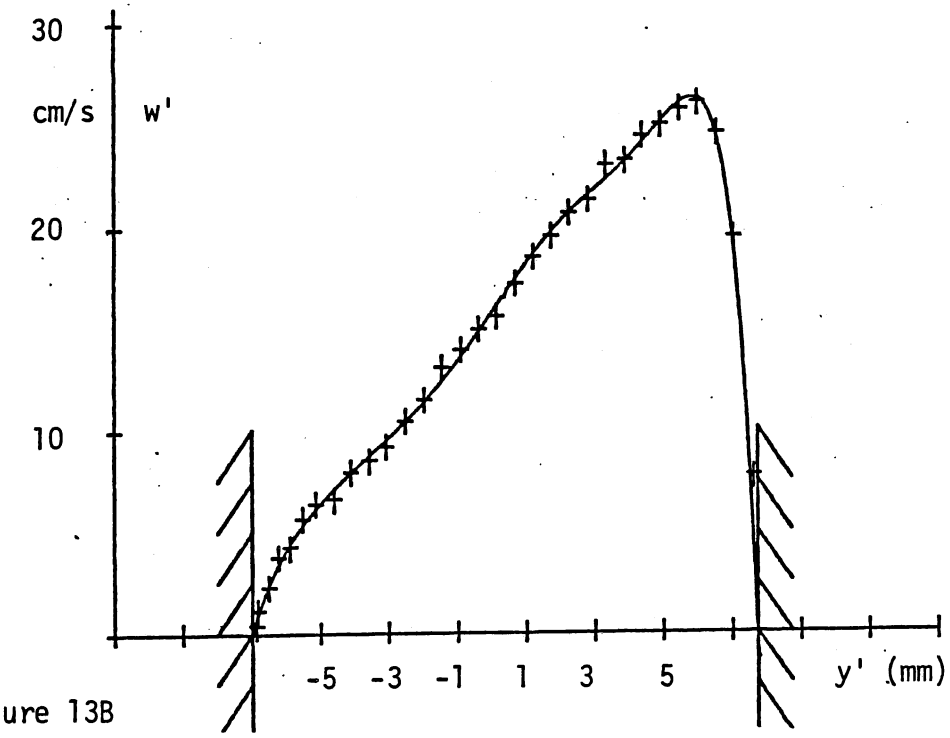

Figure 13B

Figure 13. Figure 13A shows the time averaged axial velocity component w' from series I in one of the branch tubes at x' = 2 mm and z' = 51.5 mm, while 13B is a corresponding profile at x' = 0 and z' = -51.5 mm.

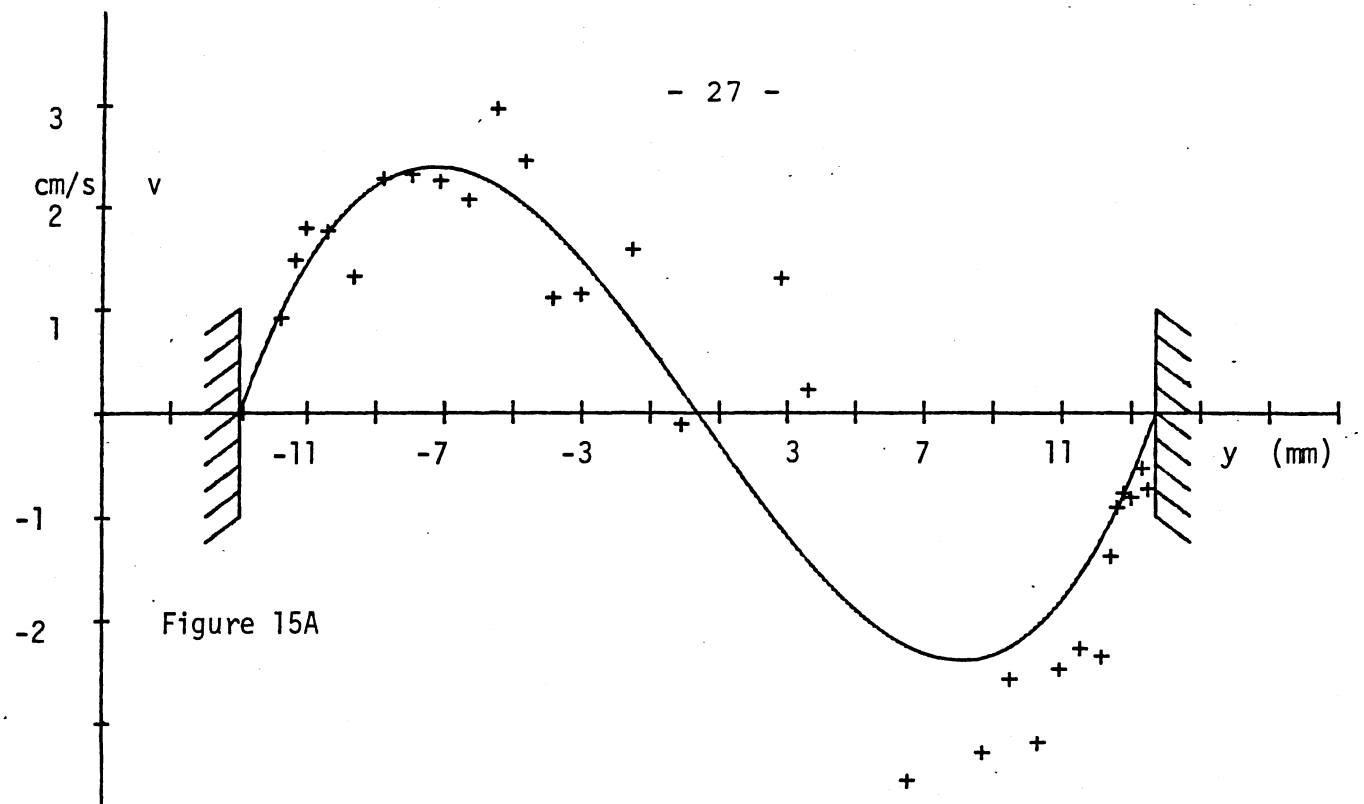

Figure 15A

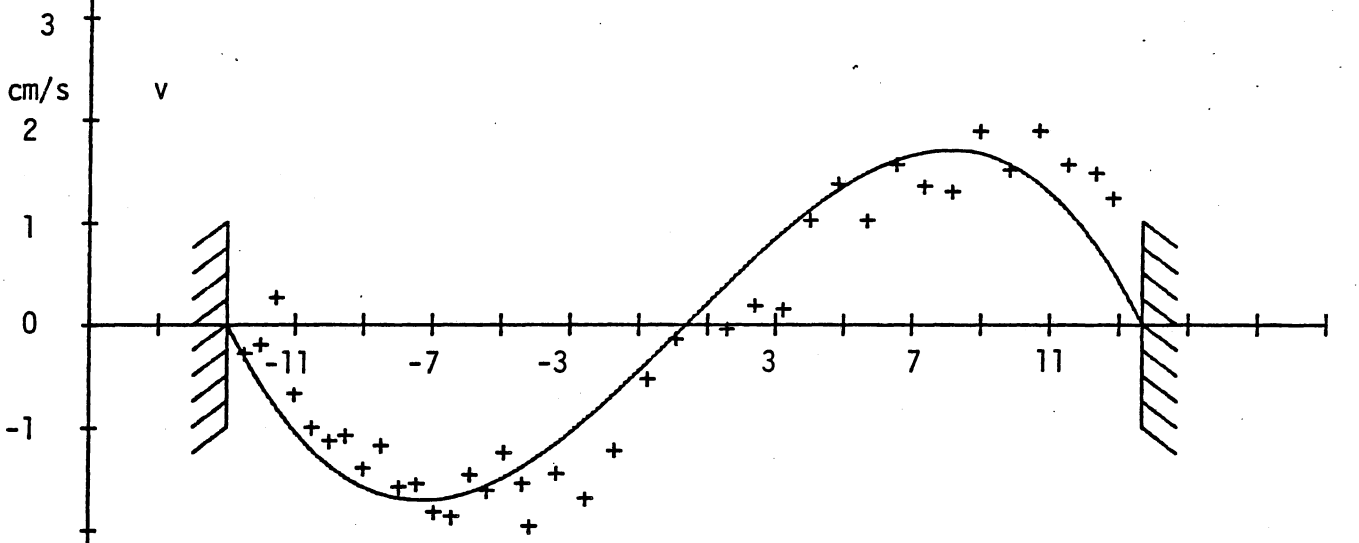

Figure 15B

Figure 15. Figure 15A shows a profile of the time averaged transverse velocity component v at z = 10 mm and x = 0 from series I, while 15B shows the correspondimg profile from series II.

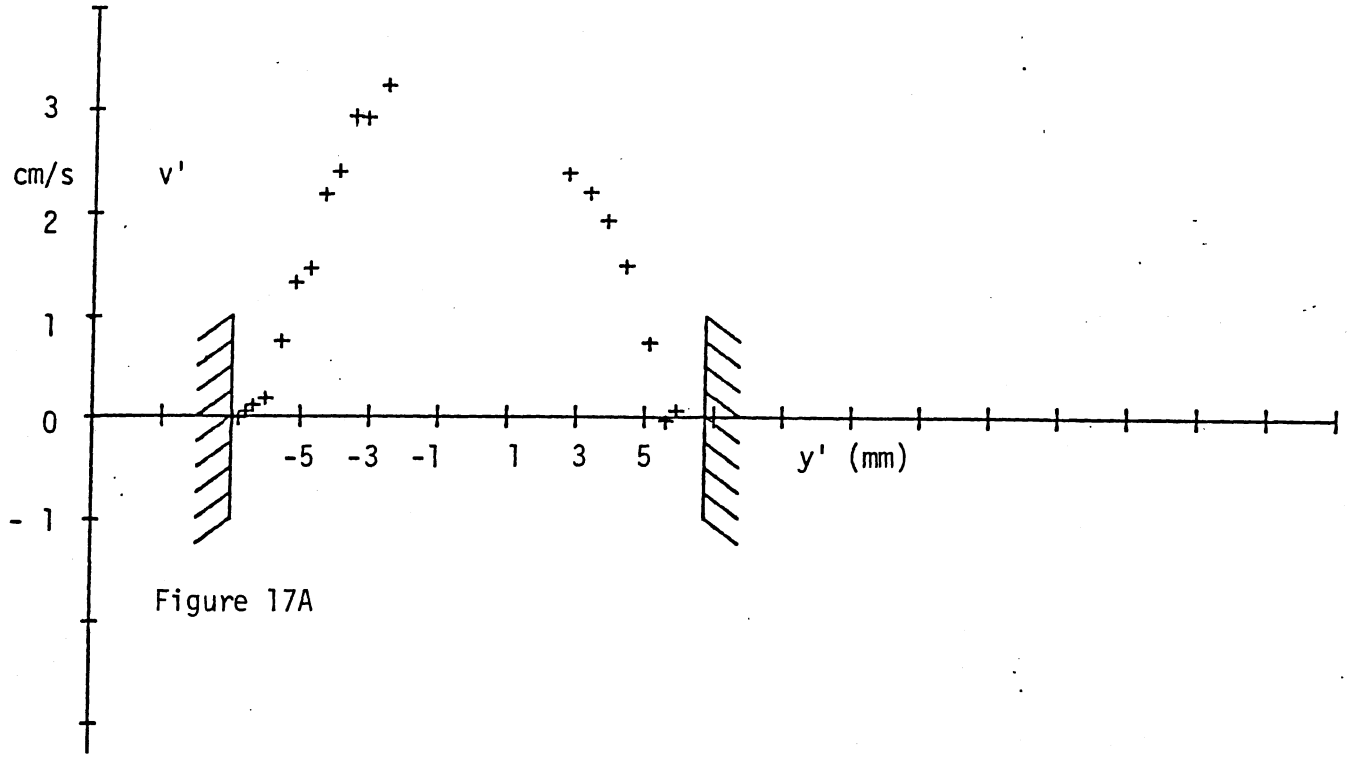

Figure 17A

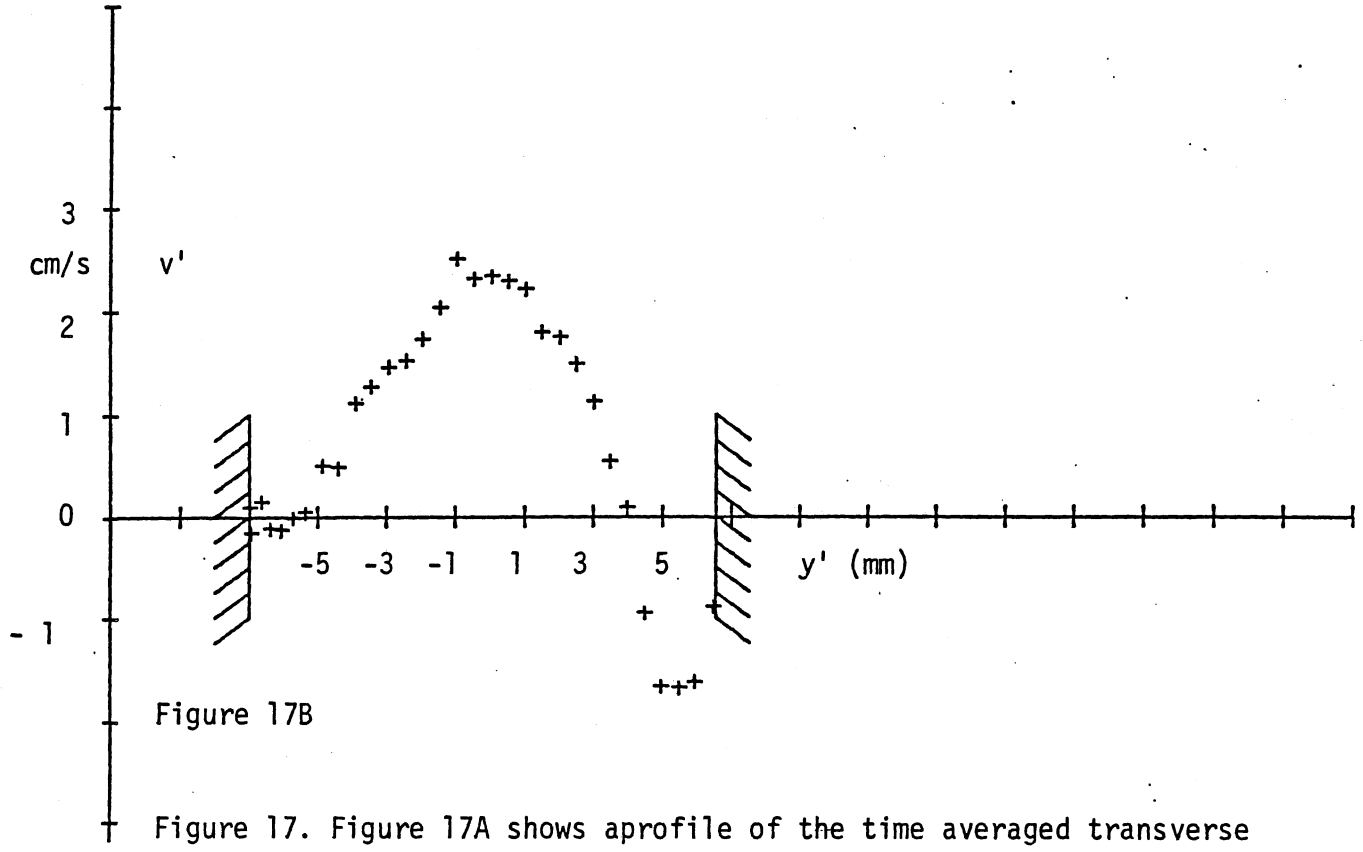

Figure 17B

Figure 17. Figure 17A shows aprofile of the time averaged transverse velocity component v' at z' = -51.5 mm and x' = 0 from series I, while 17B shows the corresponding profile from series II.

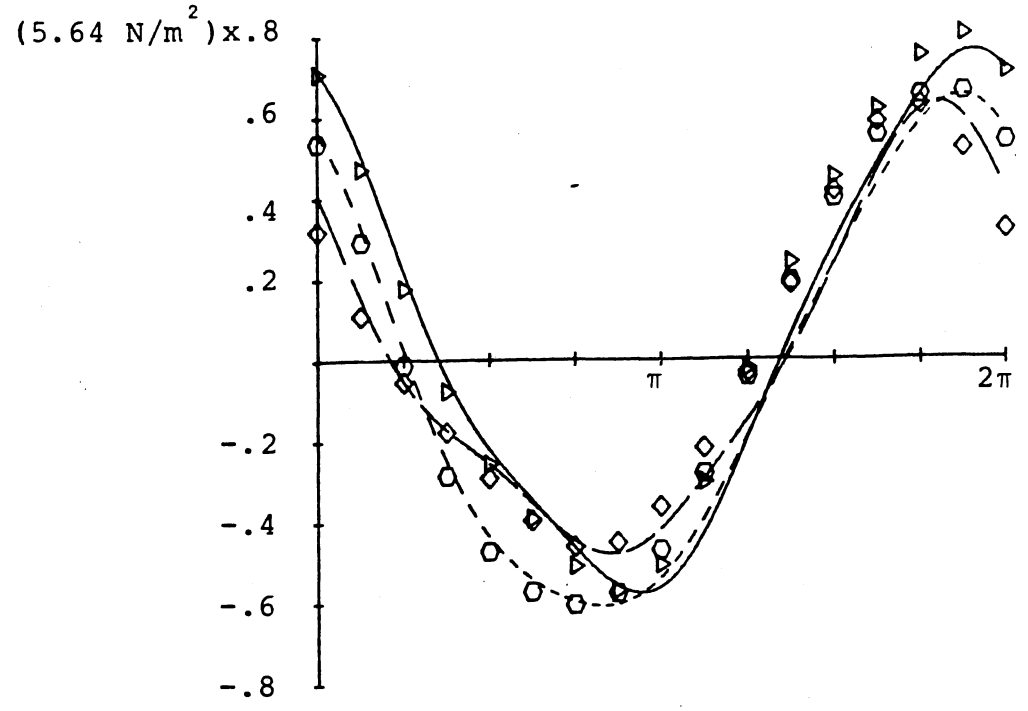

Figure 19 show wall shear stress variation in one period at x = 0 and z = -5mm (▷), z = - 20mm (◇) and z = - 50mm (○)

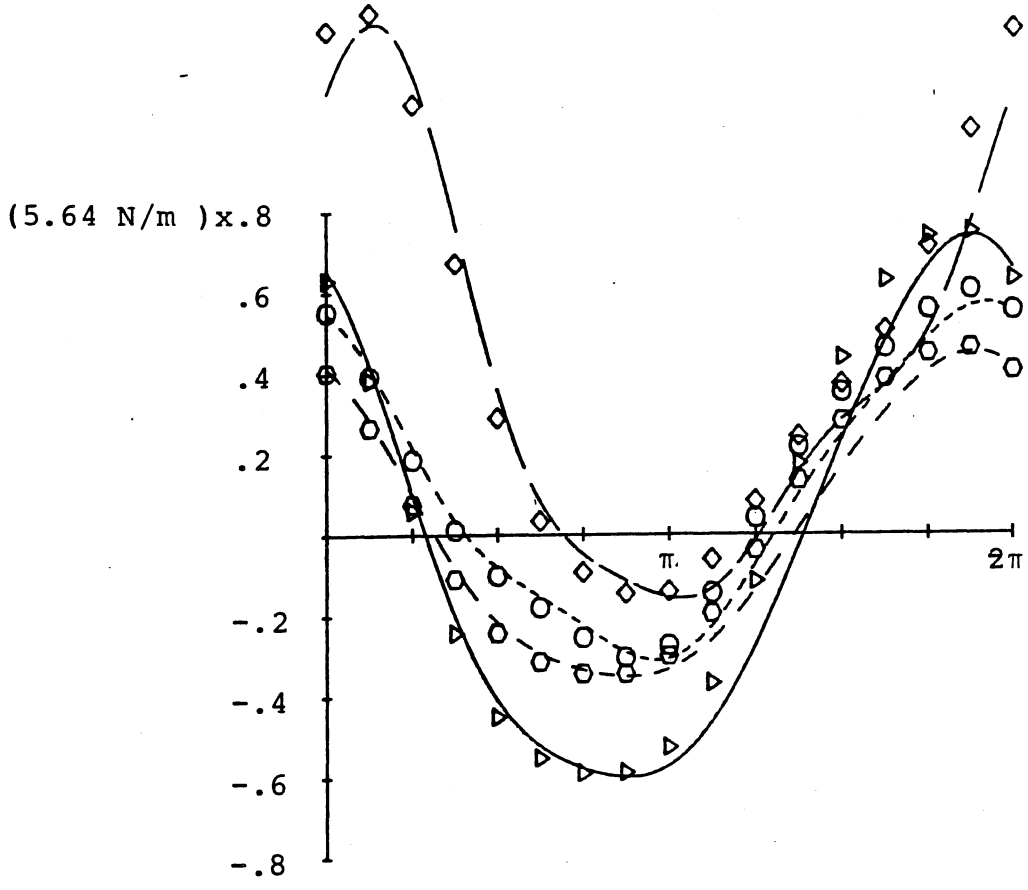

Figure 20 show wall shear stress variation in one period at x = 0 and z = - 51.5mm(▷ -outer wall, ◇ -inner wall) and z = - 38.7mm (○ -outer wall, ● -inner wall)